ChemComm

Towards Deployable Electrochemical Sensors for Per- and Polyfluoroalkyl Substances (PFAS)

Journal:	*ChemComm*
Manuscript ID	CC-FEA-05-2021-002641.R1
Article Type:	Feature Article

ARTICLE

Toward Deployable Electrochemical Sensors for Per- and Polyfluoroalkyl Substances (PFAS)

Rebecca B. Clark, Jeffrey E. Dick*

Per- and polyfluoroalkyl substances (PFAS) are an emerging class of pervasive and harmful environmental micropollutant with negative health effects on humans. Therefore, there has been extensive research into the remediation (*i.e.,* the detection, extraction, and destruction) of these chemicals. For efficient extraction and destruction, PFAS contamination must be detected at its onset; however, conventional PFAS detection methods rely on sample collection and transport to a centralized facility for testing, which is expensive and time-consuming. Electrochemistry offers a robust, inexpensive, and deployable sensing strategy that could detect pollution at its onset; however, the electrochemical inactivity of PFAS necessitates the use of a surface functionalization strategy. Molecularly imprinted polymers (MIPs) are a popular surface functionalization strategy that have been around since the 1980s for specific electrochemical detection and have expanded electrochemical detection to analytes that are not electrochemically active. MIPs have been more recently demonstrated for the detection of a variety of PFAS species, but additional advances must be made for realization of a deployable, electrochemical MIP-based sensor. This Feature highlights the history of MIPs for PFAS detection and our group's recent advances that are essential to enable the creation of a deployable electrochemical PFAS sensor: development of rigorous analytical standards to quantify interferent effects, miniaturization of the detection platform for quantification in river water, the use of ambient O_2 as the mediator molecule for detection, and the development of hardware for in-field multiplexed electrochemical sensing.

Introduction to Per- and Polyfluoroalkyl Substances

Per- and polyfluoroalkyl substances (PFAS) are an emerging and persistent class of environmental micropollutant that can be found in firefighting foams, non-stick cookware, water-resistant clothing, and personal care products.[1] PFAS have very slow biodegradation kinetics owing to the strength of their network of carbon-fluorine bonds, which have a bond dissociation energy of 546 kJ/mol.[2-4] The slow biodegradation and subsequent persistence of these chemicals have earned them the nickname "forever chemicals". Among the PFAS family, perfluorooctane sulfonate (PFOS) and perfluorooctanoic acid (PFOA), whose structures can be seen in **Figure 1,** are the most well-studied.[5, 6]

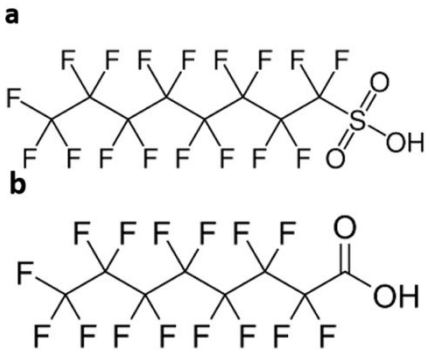

Figure 1. Chemical structure of a) PFOS and b) PFOA. Reproduced from Ref. 26 with permission from the Royal Society of Chemistry.

PFAS have been shown to have a wide variety of deleterious health effects on mammals, such as thyroid disruption, immunotoxicity, reproductive toxicity, hepatotoxicity, hypertension, among others.[7-11] Further, PFOS, PFOA, and additional PFAS have been found to exhibit many of the key characteristics of carcinogens such as altering oxidative stress, immunosuppression, and modulation of receptor mediator effects.[12] Due to these health effects and the persistence of PFAS, the United States Environmental Protection Agency (EPA) has set an advisory level for PFOS and PFOA in drinking water at 70 parts per trillion (~ 0.14 nM).[13]

The widespread prevalence and negative health effects of exposure to PFAS have sparked intense interest in research on the remediation (*i.e.,* the detection, extraction, and destruction) of these

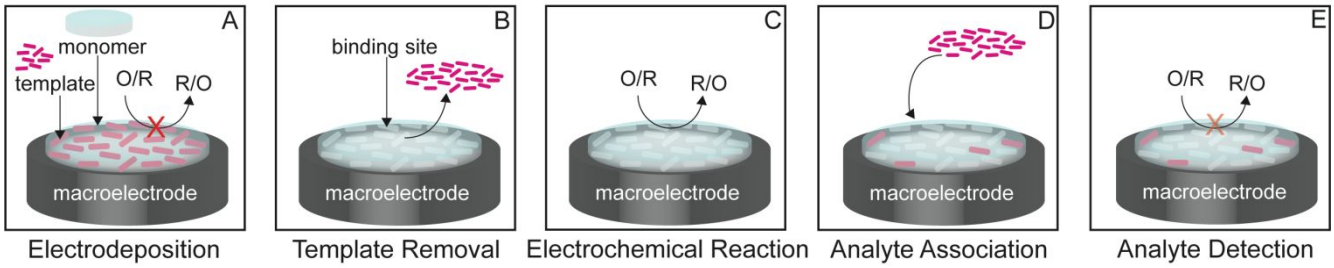

Figure 2. Schematic representation of the electrochemical detection process on a MIP-modified macroelectrode. a) Electropolymerization of the monomer in the presence of the template molecule to create the polymer on the surface of the electrode. At this point the electrochemical oxidation or reduction of the reporter molecule (represented by "O/R") is blocked. b) Wash/extraction of the template molecule from the polymer yielding binding sites in the shape of the template molecule. c) Driving of the electrochemical reaction (the oxidation or reduction of the reporter molecule, which is represented schematically by "O/R"), typically using a well-behaved, one-electron mediator on the extracted, MIP-modified macroelectrode. At this point, the electrode will have the highest number of exposed binding sites, resulting in the highest current signal. d) Association of the analyte molecule (*i.e.,* the same compound as the template molecule) *via* incubation in a solution containing the analyte molecule. e) Driving of the electrochemical reaction for detection, where the decrease in the observed current signal is proportional to the number of blocked binding sites which can be related to PFOS concentration. Adapted from Ref. 26 with permission from the Royal Society of Chemistry.

chemicals. As this article will focus on the detection of PFAS, the reader is encouraged to consult additional articles for further information on the accumulation and destruction of PFAS.[6, 14-17]

To facilitate effective remediation, PFAS contamination must be detected at its earliest onset. Conventional methods for environmental PFAS detection rely on transporting in-field water samples to a centralized facility, where chromatographic separations and mass spectrometric analysis are performed for PFAS separation, identification, and quantification; however, these methods represent a great expense, especially in the amount of time required to make a positive determination. [18, 19] More efficient, rapid, cost-effective, and deployable methods are necessary to detect PFAS at the earliest onset of environmental contamination to prevent widespread environmental exposure.

Electrochemistry is an inexpensive, robust, and portable technique that can be used to create tools for the detection of a wide variety of analytes. Perhaps one of the most useful tools developed is the glucose sensor for rapid detection of blood glucose.[20] Electrochemistry has been demonstrated for the detection of many different analytes including biomarkers[21, 22], biological entities[23], drugs[24], and chemicals[25-28], among others[29-34]. One particularly exciting modern use of electrochemical sensing is the sensing of single molecules and nanoparticles.[35-39] However, electrochemistry suffers from a central limitation in that the molecule being sensed generally needs to be electroactive (*i.e.,* the molecule can either give up an electron to the electrode surface or receive an electron). Typical electrochemical experiments monitor the current associated with the transfer of an electron from a species to or from the electrode surface. When the species of interest is unable to transfer an electron to or from the electrode surface (*i.e.,* an electrochemically inert compound) a surface-functionalization strategy must be employed. Molecularly

imprinted polymers (MIPs), which can be used for electrochemically active compounds as well[40-42], are a widely used surface-functionalization strategy for the detection of electrochemically inactive compounds *via* an indirect detection method.

For indirect detection, a secondary molecule, termed a mediator molecule, which can be readily oxidized or reduced is used for the detection of the analyte. As the analyte interacts with the surface of the electrode, the current passed from the oxidation or reduction of the mediator molecule will decrease, enabling the signal associated with the mediator molecule's oxidation or reduction to be used for the indirect detection of the analyte. This process is depicted in detail in **Figure 2**. A monomer is electropolymerized at the surface of a macroelectrode in the presence of a template molecule, as shown in Figure 2a. At this point the surface of the electrode is blocked so the electrode is unable to oxidize or reduce the mediator molecule. The mediator molecule is depicted as O/R in the figure because it could either be oxidized or reduced. While our lab has typically used *o*-phenyldiamine (*o*-PD), we note here that *o*-PD is not the only polymer with which one can form MIPs.[43-46] A treatment step (generally a wash with a 50:50 water/methanol solution) is used to extract the template, leaving a template-removed electrode with empty binding sites (Figure 2b). Previously, our lab has used x-ray photoelectron spectroscopy to confirm template extraction of the template molecule when PFOS was used as the template molecule by considering the fluorine 1s peak.[26] An electrochemical reaction, typically using a laboratory-grade, well-behaved one-electron mediator, is then driven on the template-removed sensor, as shown in Figure 2c. Previous reports have driven the oxidation of a ferrocene derivative, such as ferrocenecarboxylic acid[27], ferrocene methanol[28], ferrocyanide[47], or vinyl ferrocene.[48] In the presence of the template molecule, template molecules will associate with the MIP (Figure 2d) and block the electrochemical signal (Figure 2e). As the concentration of associated template molecules increases, the surface area of the electrode decreases. No matter what electrochemical technique (for the purpose of this manuscript, impedimetric & voltammetric) is chosen, the decrease in electrode surface area due to template binding will affect the electrochemical signal in a proportional way. The technique shows extraordinary analytical sensitivity, as it it able to detect changes at the sub-ppt (nM) level.

The association of template molecules in the binding sites of the MIP follows the Langmuir binding isotherm.[25-27] As the concentration of associated template molecules increases, the observed current decreases, providing a binding isotherm and associated calibration curve relating the electrochemical signal to the concentration of the template molecule. It is worth pointing out the main assumptions behind using the Langmuir model to fit such binding curves. The Langmuir model assumes binding sites do not interact. The derivation of the change in current with concentration of PFAS species requires one to assume that each individual binding site behaves like a nanoelectrode without diffusional coupling to other binding sites. Because the bulk voltammogram of the template-removed MIP often yields a cyclic voltammogram with a peak response (as opposed to a limiting, horizontal response), this assumption is not quite accurate. Even so, the Langmuir model fits the data with high accuracy and can be used to robustly compare association constants across a variety of template molecules and potential interferents on a relative basis.

MIP-based sensing strategies offer the capability of creating a sensitive and selective electrochemical detection strategy for the electrochemically inert group of PFAS chemicals; however, for efficient detection the sensing platform also needs to be deployable (*i.e.,* avoiding the use of laboratory-grade mediators that are not present in the environment and the development of the hardware for taking the measurements in deployable settings). This article will focus on the groundwork laid for MIP-based

PFAS detection and our group's work on developing a robust analytical method to evaluate PFAS binding on MIPs, miniaturized MIPs for detection in river water, methods to use ambiently available oxygen for the sensing modality, and methods to multiplex sensing in relevant environmental matrices.

MIP-Based PFAS Detection:

Laying the Groundwork: First Report of Electrochemical PFOS Detection *via* MIP-Modified Electrodes

PFOS detection *via* a MIP-based electrochemical sensor was first demonstrated in 2018 by Ugo and co-workers.[27] A molecularly imprinted polymer that used *o*-PD and PFOS as the monomer and template molecule, respectively, was generated on a gold macroelectrode. Using the decrease in signal from the oxidation of ferrocene carboxylic acid *vs*. the concentration of PFOS, a calibration curve from 0.1 nM to 1.5 µM was created showing the successful detection of PFOS in ammonia buffer (pH = 8.4). The calibration curve showed two distinct linear regions from 0.1 to 4.9 nM and 9.5 nM to 1.5 µM, and yielded a detection limit of 0.04 nM, which is below the 0.14 nM limit set forth by the United States Environmental Protection Agency. Further, the developed sensor showed < 10% change in performance in the presence of the following interferents, which have similar structures to PFOS: dodecylbenzenesulfonic acid (DBSA), perfluorooctanoic acid (PFOA), perfluorohexanoic acid (PFHxA), and perfluorohexanesulfonic acid (PFHxS).

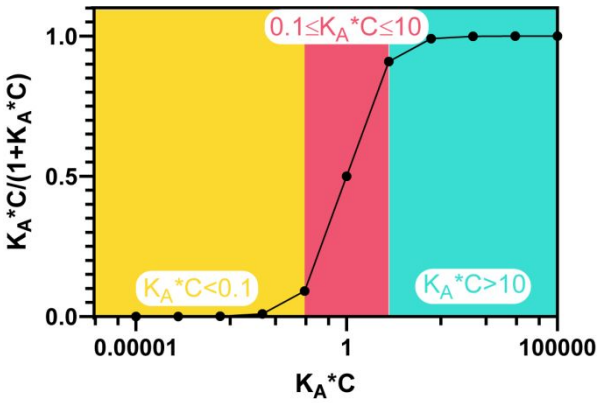

Figure 3. Graphical representation of the general form of the Langmuir Binding Isotherm (Equation 1). The extremely sensitive linear region can be observed when the product of $\boldsymbol{K_A C}$ is between 0.1 and 10.

It should be noted that the calibration curve they presented, as well as the ones we will present in subsequent sections, present the data as a semi-log plot. Recently, the use of semi-log plots was appropriately called into question.[49] While plotting such data has a long standing tradition in the MIP-based detection literature[25-28], we would like to point out that there is a mathematical justification for using a semi-log plot to describe calibration curves for binding processes, such as the association of template molecules into a MIP. The general form of the Langmuir isotherm[25] is given by the following equation:

$$\frac{\boldsymbol{K_A C}}{\boldsymbol{1 + K_A C}} \qquad \text{Equation 1}$$

Where $\boldsymbol{K_A}$ is the association constant and $\boldsymbol{C}$ is the concentration of template molecule. The logarithm of this function reveals a sigmoidal curve and yields a highly sensitive linear region when the product, $\boldsymbol{K_A C}$, is between 0.1 and 10 (**Figure 3)**. Previously, we have shown the $\boldsymbol{K_A}$ for PFOS binding on such templates is ~10^{13} cm^3/mol.[25] Considering the concentration range used in the studies reported in this article, a semi-log plot is an appropriate method to report such binding data because $\boldsymbol{K_A C \sim 1}$. This

distinction should be considered (and justified) in how past and future data have been and are presented. One may also interpret the resulting sigmoidal shape from above as three linear regions (two insensitive regions and one more sensitive region about 1). This explains why groups have observed more than one linear region, each with a different sensitivity.[25, 27, 28, 50]

The work done by Ugo and co-workers was the first innovation in the path that is leading towards a deployable electrochemical sensor for PFAS. This initial work inspired many additional questions: What binding isotherm model is correct? How does one robustly characterize interferent effects? Can PFAS be quantified in relevant matrices like river water without salt additives? Can similar data be obtained without the addition of expensive, well-behaved, one-electron mediators? Can such measurements be deployed and eventually multiplexed? How does one gain robust selectivity with MIP-based sensors? Because the answers to these questions can be used to develop a robust tool (*i.e.,* a deployable sensor) of great use to humanity, our group began working to find answers. In the sections that follow, we outline our work in addressing the above questions.

What binding isotherm model is correct?

While Ugo and colleagues provided groundwork, their equation for the binding isotherm has unequal units on each side of the equal sign.[27] This motivated us to derive a more robust equation for the change in current with concentration of PFAS molecule, provided below[25]:

$$\boldsymbol{i_o - i = \frac{(BS)_0[PFAS]K_A}{1 + [PFAS]K_A} * 4nFDC^* r} \qquad \text{Equation 2}$$

Where i_o is the initial peak current (*i.e.,* in the absence of a PFAS molecule), i is the current in the presence of PFAS, $(BS)_0$ is the total number of binding sites, [PFAS] is the concentration of PFAS, K_A is the binding affinity, n is the number of electrons involved in the electrochemical reaction, F is Faraday's constant, D is the diffusion coefficient of the electroactive species,

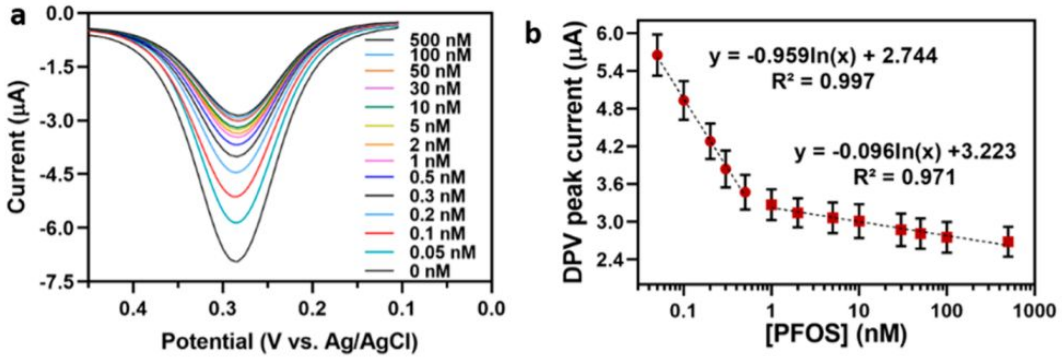

Figure 4. a) DPV responses of a MIP-modified glassy carbon macroelectrode in 0.5 mM ferrocene carboxylic acid solution obtained following 15 min incubations in a solution with increasing concentrations of PFOS. b) Dependence of the DPV peak current on PFOS concentration. Reproduced from Ref. 25 with permission from the Royal Society of Chemistry.

*C** is the bulk concentration of the electroactive species, and *r* is the radius of the electrode (in this case the radius of a PFOS molecule, as each binding site was treated as an individual microelectrode). This equation provides a more accurate framework to begin quantifying selectivity for MIP-based sensors. One important assumption in the derivation of the above equation is that each binding site acts as its own nanoelectrode, where the radius is taken to be that of the template molecule. If this is true, a cyclic voltammogram of a well-behaved electron mediator in the template-extracted MIP should show a sigmoidal shape because the diffusion layers of neighbouring binding sites will not overlap. In reality, while the voltammogram is more sigmoidal than the bare macroelectrode, peaks are observed.[25] Despite this assumption, and as seen in **Figure 5**, the Langmuir model matches the results remarkably well and can serve to relatively compare potential interferent molecules. One way to mitigate diffusion layer overlap in such measurements is by using pulse voltammetry at a high enough frequency (*vide infra*).

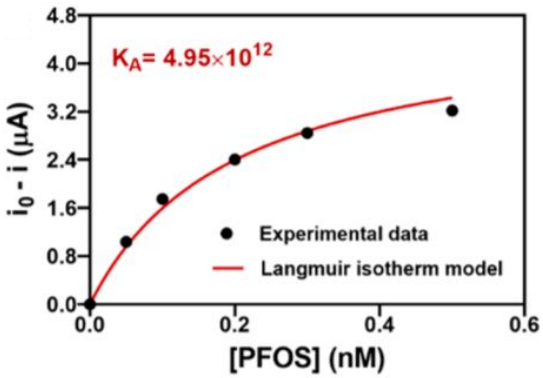

Figure 5. Binding isotherm of the MIP-modified glassy carbon macroelectrode representing the correlation between changes in DPV responses and PFOS concentration ranging from 0 to 0.5 nM. The binding affinity is in units of $\mathrm{cm}^3/\mathrm{mol}$. Reproduced from Ref. 25 with permission from the Royal Society of Chemistry

How does one robustly characterize interferent effects?

As one of the long-standing limitations of MIPs is their limited selectivity[51, 52], it is necessary to better understand and characterize interferent effects. To investigate this, our lab probed the response of a PFOS-templated, MIP-modified macroelectrode towards the targeted analyte (PFOS) and a variety of other relevant interferents (humic acid, sodium chloride, and alternate PFAS). The electrode was modified with a MIP which used *o*-PD and PFOS as the monomer and template molecule, respectively, on a glassy carbon macroelectrode (*r* = 1.5 mm).[25] Prior to investigation of the interferent effects, the sensor's performance towards PFOS was investigated. Similar to the work presented by Ugo and co-workers, we used differential pulse voltammetry to monitor the signal from the oxidation of ferrocene carboxylic acid

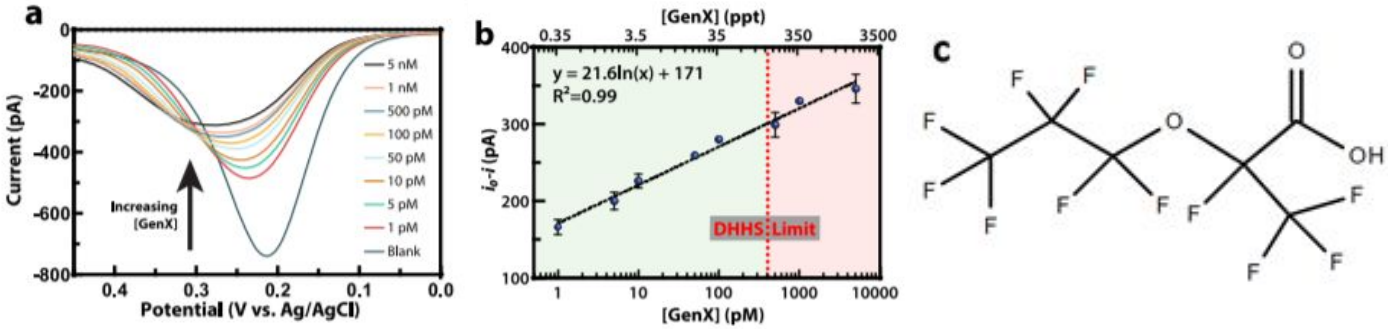

Figure 6. a) DPV response showing a decrease in the oxidative current due to the blocking of surface sites within the MIP-modified electrode by increasing concentrations of GenX. The shift in the peak potential is possibly caused by charge or mass transfer effects due to the interactions of the analyte with the MIP. A MIP-modified Au microelectrode, a Ag/AgCl wire, and a platinum coil were used as the working, reference, and counter electrodes, respectively. b) Calibration curve showing the dependence of oxidative peak current as a function of GenX concentration. N = 3 individual sensors. c) Structure of GenX. Reproduced from Ref. 28 with permission from the Royal Society of Chemistry.

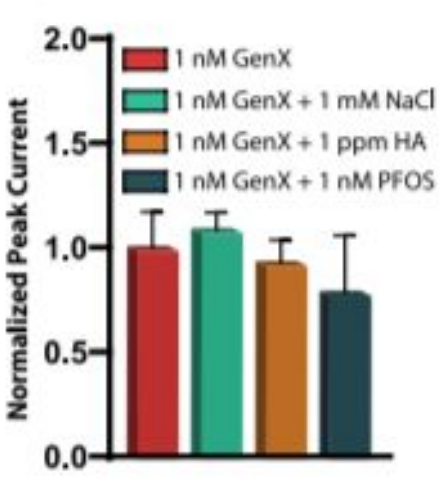

Figure 7. Effect of interferent species such as NaCl, humic acid (HA), and perfluorooctanesulfonate (PFOS) on the MIP detection efficiency. In all cases, the addition of interferent species caused a statistically insignificant change (Brown–Forsythe analysis of variance) in the performance of the sensor for the detection of 1 nM GenX. N = 3 individual sensors. Reproduced from Ref. 28 with permission from the Royal Society of Chemistry.

in response to incubating the MIP-modified electrode in increasing concentrations of PFOS. The MIP-modified electrode was incubated for 15 minutes in an appropriate concentration of PFOS in ammonium buffer prior to obtaining the differential pulse voltammogram. The differential pulse voltammograms illustrate a consistent decrease in the peak current in response to increasing concentrations of PFOS in ammonia buffer (**Figure a**). The resulting calibration curve showed two distinct linear regions from 0.05 to 0.5 nM and 1 to 500 nM and had a LOD of 0.05 nM, which is lower than the 0.14 nM advisory limit provided by the Environmental Protection Agency (**Figure 4b**).

We then chose to investigate the behavior of the MIP-based sensor towards PFOS and the various chosen interferents. As the ultimate goal of the research is the creation of a deployable electrochemical sensing strategy (*i.e.,* for use in natural waterways such as river water), the interferents chosen were ones commonly found in river water (*i.e.,* humic acid, sodium chloride, and the additional PFAS species: perfluorooctane sulfonate (PFOS), perfluorooctanoic acid (PFOA), and perfluorobutanesulfonic acid (PFBS)). Binding affinities of the MIP towards the PFOS and the various interferents were determined by fitting experimental data to a Langmuir binding isotherm model according to Equation 2. Similar to the previously described PFOS experiments, differential pulse voltammetry was used to monitor the signal observed from the oxidation of ferrocene carboxylic acid in response to increasing concentration of analyte; however, in this case, the analyte was one of the interferents.

We fit the [PFOS] region from 0.05 to 0.5 nM of the curve presented in **Figure 4b** to the Langmuir Binding Isotherm model and obtained a binding affinity of $\mathbf{4.95x10^{12}\frac{cm^3}{mol}}$ (**Figure 5**). This value provided a baseline for comparison for the other PFAS species and interferents investigated. The determined binding affinities for humic acid and chloride, both common river water interferents, were roughly a million times lower than that of PFOS at $\mathbf{6.01\ x\ 10^5\frac{cm^3}{mol}}$ and $\mathbf{9.05\ x\ 10^7\frac{cm^3}{mol}}$, respectively. The determined binding affinities for the alternate PFAS species PFOA and PFBS were very similar to PFOS at $\mathbf{3.41\ x\ 10^{12}\ \frac{cm^3}{mol}}$ and $\mathbf{1.43\ x\ 10^{13}\frac{cm^3}{mol}}$, respectively. While these results show promise for the selectivity of a fluorinated compound (*i.e.,* a PFAS species over a non-fluorinated compound), they also highlight the limited selectivity between PFAS species and subsequent need for further research on the topic. The selectivity between PFAS species is of critical importance to a deployable PFAS sensor as it enables a more thorough understanding of the transport of the different species in the environment which can enable better remediation efforts. With a more thorough understanding of interferent effects, our lab continued forward to answer questions related to the detection of PFAS in relevant matrices. Attaining selectivity is the 'elephant in the room' and remains our most significant area of focus moving forward.

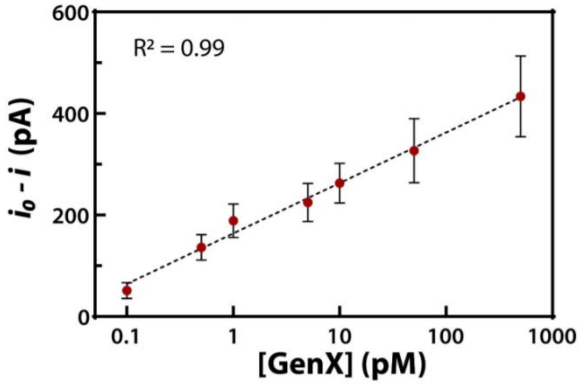

Figure 8. Calibration curve showing the dependence of oxidative peak current as a function of GenX concentration in water samples collected from the Haw River using the ferrocene methanol detection strategy. These water samples are highly resistive (8.4 kΩ˙cm), warranting the use of microelectrode sensors to reduce signal distortion due to iR-drop. N=4 individual sensors. Reproduced from Ref. 28 with permission from the Royal Society of Chemistry.

Can PFAS be quantified in relevant matrices like river water without salt additives?

By 2019, the published work, both by our group and others, presented has focused on PFAS detection in laboratory-generated buffers. As the ultimate goal is to be able to use the sensor in natural waterways, the question of whether or not PFAS could be quantified in relevant matrices (*e.g.,* river water) had to be addressed. One challenge to overcome in river water is that the resistivity is higher than ocean water. Resistance warps electrochemical data by introducing *i*R drop. One way to decrease the influence resistance has on the electrochemical response is to use smaller electrodes. Smaller electrodes pass a smaller current in the same voltage regime, decreasing the effect of solution resistance. Our group was among the first to miniaturize MIP-based sensing strategies to ultramicroelectrodes for detection purposes (so-called μ-MIPs). We chose to investigate the detection of GenX, whose structure can be seen in **Figure 6c**, because it is becoming increasingly prevalent in the environment. GenX is commonly used as replacement for PFOA in the production of fluorocarbon products, due to the extensive regulations placed on PFOA.[28] Prior to investigation in river water, the detection was first validated in ammonia buffer. Similar again to the aforementioned experiments, the oxidative signal, this time of ferrocene methanol, was monitored in response to increasing concentrations of GenX in ammonia buffer.

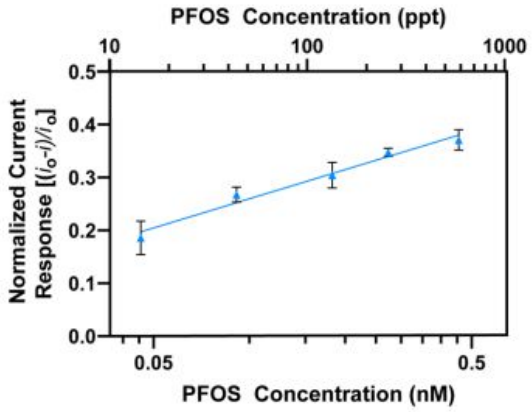

Figure 9. Calibration curve in Haw River water illustrating the dependence of normalized current response, (*i*o − *i*)/*i*o, on the natural log of PFOS concentration with the x-axis on a logarithmic scale. The equation of best fit was y = (0.079 ± 0.005) ln (x) + (0.436 ± 0.009) and the R^2 value was 0.9758. Reproduced from Ref. 26 with permission from the Royal Society of Chemistry.

The differential pulse voltammograms showed a consistent decrease in response to the increasing concentration of GenX (**Figure 6a**). The resultant calibration curve showed a linear region from 1 pM to 5 nM and a limit of detection of 250 fM (**Figure 6b**). Of note, the North Carolina Department of Health and Human Services put a provisional limit on the concentration of GenX in water at 140 ppt which is marked on the calibration curve to illustrate the environmental relevance of this technique. The sensor also showed a robust signal in the presence of three common interferents (chloride, humic acid, and PFOA) with there being no statistical change in the sensor's

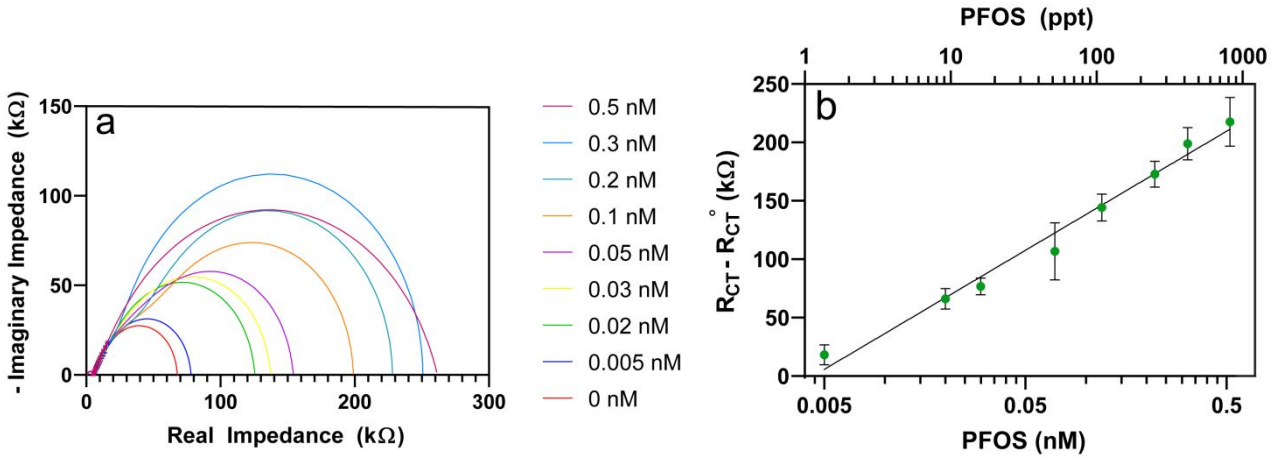

Figure 10. a) Overlay of the experimental data (represented by the x's) and simulated Nyquist plots using the resistance and capacitance values determined by fitting the experimental Nyquist plots to the equivalent circuit. The resistance to charge transfer is equal to the width of the large semicircle. b) Linear calibration curve showing the dependence of the normalized resistance to charge transfer on the natural log of PFOS concentration realized by taking a semilog plot of the associated isotherm. The line of best fit was y = (44 ± 3) ln (x) + (240 ± 18), and the R^2 value was 0.9825. N=3 individual sensors. Reproduced from Ref. 26 with permission from the Royal Society of Chemistry.

response towards GenX in the presence or absence of the interferent (**Figure 7**). As GenX is a smaller molecule than PFOS, size exclusion from the binding sites may be a contributing factor to the sensor's selectivity for GenX over PFOS.

After validating the use of the sensor in ammonia buffer, the sensor's performance was investigated using river water samples from the Haw River in North Carolina (35.77585654738046º, -79.1467275350264º latitude, longitude) as the sample matrix. Similar to the GenX experiments performed in ammonia buffer, the oxidative signal from ferrocene methanol was monitored with a MIP-modified gold microelectrode in response to increasing concentrations of GenX; however, this time the measurements and incubations were performed in river water. A calibration curve showing the successful detection of GenX in river water was obtained between 0.1 to 500 nM, which again contained the DHHS limit from the state of North Carolina (**Figure 8**). This work provides a key advancement towards the overarching direction of the research towards a deployable sensor as we have now demonstrated the detection of a PFAS species in river water, one of the relevant matrices for deployable detection, without any salt additives; however, the addition of laboratory-grade, well-behaved one-electron mediators still needs to be alleviated.

<u>Can similar data be obtained without the addition of expensive well-behaved, one-electron mediators?</u>

Oxygen, which is more commonly seen as a hinderance in electrochemical studies, provided a promising alternative for use as the electron mediator, as it is readily available in natural waterways under ambient conditions.[53] Our lab investigated the detection of PFOS *via* differential pulse voltammetry on a MIP-modified glassy carbon macroelectrode (r = 1.5 mm), where the MIP was generated using *o*-PD and PFOS as the monomer and template molecules, respectively; however, instead of monitoring the oxidative signal of a ferrocene derivative, we chose to use the reductive signal of oxygen instead.[26] Further pushing

the field towards deployable sensing, we performed the experiments in river water from the Haw River in North Carolina. Using differential pulse voltammetry to monitor the oxygen reduction reaction, PFOS was able to be successfully detected in river water with a concentration range of 0.05 to 0.5 nM, which contains the environmentally relevant EPA limit of 0.14 nM (**Figure 9**); however, the differential pulse voltammograms were subject to peak shifting and shouldering, attributed mainly to oxygen's solubility in non-imprinted regions of the polymer, which lead to recording the current response at an arbitrary, irreproducible potential. This limitation observed from using oxygen reduction with differential pulse voltammetry led us to investigate electrochemical impedance spectroscopy as an alternative technique.

Electrochemical impedance spectroscopy, which is especially sensitive to changes at the surface at of the electrode, was investigated because we hypothesized that the association of the template would increase the charge transfer resistance to oxygen reduction due to the following relationship[54]:

$$R_{CT} = \left(\frac{RT}{F}\right)\frac{1}{i_0} \qquad \text{Equation 3}$$

Where R_{CT} is the charge transfer resistance, R is the universal gas constant, T is temperature, F is Faraday's constant (RT/F has units of volts, V), and i_0 is the exchange current, which is proportional to the electrode area. Thus, as PFOS molecules bind to the binding sites, the overall effective electrode area decreases, and the smaller exchange current increases the charge transfer resistance to oxygen.

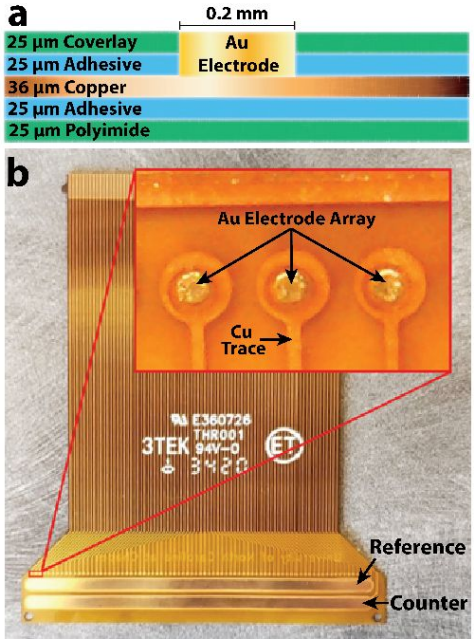

Figure 11. a) Cross-section schematic showing various layers of the flexible printed circuit electrode array and their respective thicknesses. (b) Image of the fabricated flexible printed circuit array with a magnified image of three working electrodes. Reproduced from Ref. 55 with permission from the Royal Society of Chemistry.

As we hypothesized, the resistance to charge transfer did indeed increase with increasing concentrations of PFOS (**Figure 10a**). Unlike the monitoring of the oxygen reduction reaction with differential pulse voltammetry, where the current response was recorded at an arbitrary potential, the resistance to charge transfer could be clearly determined *via* the diameter of the large semicircle on the Nyquist plot (**Figure 10a**). The variation in the height of the semicircle, particularly evident in the plot of 0.5 nM PFOS, is attributed to changing capacitance at the MIP's surface as more PFOS molecules associate with the MIP.[54] The resultant calibration curve showed a linear range from 0.005 to 0.5 nM, which expanded the range observed with differential pulse voltammetry and still included the Environmental Protection Agency limit of 0.14 nM (**Figure 10b**). As with the previously reported experiments, we observed no statistical change in the sensor's response toward PFOS in the presence of humic acid and chloride. These results represent an essential step forward in the field of deployable PFOS sensing with an electrochemical sensor, as the measurement has been demonstrated in the relevant matrix (*i.e.,* river water) without salt additives or the use of expensive, well-behaved one-electron mediators. The

next essential step that must be taken is developing the physical means of taking these measurements in a multiplexed fashion to enable proper statistical analysis to ensure accuracy (and versatility) with a deployable sensor. Motivated by the necessity of this next step, our group began developing the required hardware for multiplexed electrochemical detection modalities.

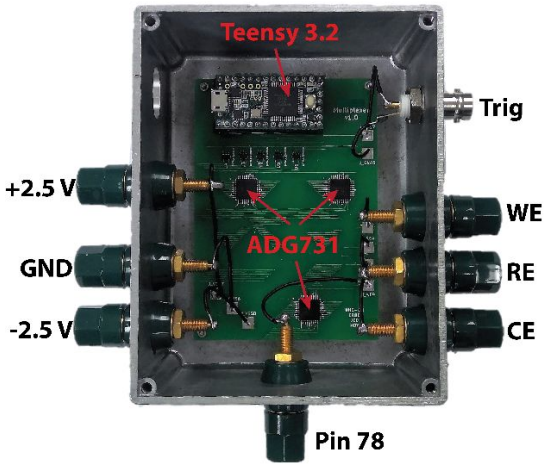

Figure 12. Multiplexer interface inserted into a metal enclosure. The WE, CE, and RE are interfaced to an external potentiostat (not shown), while the FPC electrode array connects to the connector on the bottom of the PCB at a right angle (orthogonal). Reproduced from Ref. 55 with permission from the Royal Society of Chemistry.

Can such measurements be multiplexed?

The field of MIP-based electrochemical sensors for PFAS has taken significant strides towards becoming a deployable alternative to the current process of taking water samples to a centralized facility for chromatographic and spectrometric analysis. Our demonstration of the technology's ability to be used in water samples from natural waterways and without salt additives or the use of laboratory-grade chemicals has propelled the chemistry to a point where deployable sensing is feasible. To enable efficient and accurate deployable sensing, we have been working on developing a physical means for taking the measurements in the environment, consisting of two critical pieces of hardware: an electrode array and a means of connecting the electrode array to a potentiostat for multiplexed analysis (*i.e.,* a multiplexer).[55] The electrode array still provides the same advantages of a single macro- or microelectrode, while also enhancing spatial resolution and providing higher sensitivity and/or precision.[56] Further, the electrode array would enable statistical analysis of results (by imprinting multiple electrodes with the same PFAS) and the detection of multiple PFAS species (by imprinting different electrodes with different PFAS), provided that each electrode can be individually addressed. To take measurements, the electrode array must be able to be interfaced with a potentistoat. One can interconnect all the electrodes of the array to the same potentiostat and take an average signal, connect each electrode to an invdidual potientiostat/use a multi-channel potentisotat, or use interfacing hardware that enables switching between each electrode on the array. [57-59] The interfacing hardware (*i.e.,* a multiplexer) is best suited for electrode arrays with a large number of electrodes, as it can be connected to any potientiostat, enables the electrodes to be individually addressed, and does not require dedicated circuity for each electrode.

Towards the goal of developing the necessary hardware, we developed both the electrode array and multiplexer (*i.e.,* the means of connecting the electrode array to the potentiostat).[55] A flexible printed circuit electrode array containing 78 gold working electrodes, gold counter, and gold quasi reference electrode was designed with KiCad software and fabricated by Epec Engineered Technologies (**Figure 11**). The electrodes are all composed of gold-plated copper, and successful plating of gold was confirmed by the absence of copper signal in background cyclic voltammetry and Scanning Electron Microscopy (SEM) with Energy Dispersive X-Ray Analysis (EDX).[55] The developed electrode array possesses the capability of

being used for the aforementioned needs for both multiple measurements of the same analyte and measurement of multiple analyte species.

For multiplexed measurement with the electrode array, we developed a universal multiplexer (a means of connecting the chip to any potentiostat) which enabled the individual addressing of each electrode and was simply termed the "multiplexer" (**Figure 12**). The multiplexer was demonstrated to make successful connection and measurements at all 78 electrodes without altering the electrochemical performance of the electrodes.[55] The development of this hardware fulfills the ultimate step towards bringing the bench top chemistry developed for deployable detection (*i.e.,* detection in natural waterways without the addition of salts or a well-behaved mediator) to a platform that can be used to realize in-field deployable monitoring of environmental contaminants.

Conclusions and Future Directions: How does one deploy and gain robust selectivity with MIP-based sensors?

Building off the groundwork provided by Ugo and co-workers, our group has continued to push the field of MIP-based electrochemical sensors forward and towards use as a deployable sensing strategy. We have developed robust methods to quantify interferent effects, demonstrated PFAS detection in complex matrices (*i.e.,* river water), moved away from the use of well-behaved, one-electron mediators, and have developed the necessary hardware for the deployable multiplexed detection of multiple analytes of interest. Further, we have demonstrated the reproducibility of the method through repeat trials and selectivity of the MIP-based sensor by demonstrating its statistically similar response to the analyte of interest in the presence and absence of relevant interferents.

The work our group has done has provided many advancements towards deployable MIP-based sensing; however, as in most scientific endeavors, there is still plenty to do. Selectivity between PFAS species remains an issue that needs to be solved and is a main area of focus for our lab going forward. Using the developed hardware presented in this paper, our other main focus is optimizing and demonstrating deployable PFAS detection in the environment through connecting the multiplexer and MIP Chip to a cheap and portable potentiostat. Many groups[60, 61], including ours[62] have developed these potentiostats, and one of our next directions is using the multiplexer in conjunction with the Sweepstat (*i.e.,* the portable potentiostat) that our lab created. The future combination of the multiplexer, MIP Chip, and portable potentiostat will make this sensing platform readily available to citizen scientists. Additionally, the long-term stability of the hardware and the MIPs on the MIP Chip will be investigated and optimized for deployable use. The continued research on these topics will further advance the field of MIP-based sensors and can provide a robust tool of great use to humanity.

Author Contributions

RBC and JED wrote the manuscript.

Conflicts of interest

There are no conflicts to declare.

Acknowledgements

We are grateful to the Department of the Army, United States Army Engineer Reearch and Development Center (ERDC) for supporting this work under cooperative agreements W912HZ1920018 & W912HZ2020063. This work would not have been possible without the hard work of several current and former postdoctoral scholars, graduate students, undergraduate students, and research support. In particular, we would like to acknowledge Rezvan Kazemi, Ph.D (University of North Carolina at Chapel Hill), Matthew W. Glasscott, Ph.D (Engineering Research and Development Center), Emili I. Potts, B.S. (University of North Carolina at Chapel Hill), Jenna C. DeMartion (University of North Carolina at Chapel Hill), and Matthew D. Verber, M.S. (University of North Carolina at Chapel Hill) for laying the foundations for this work in our laboratory. We would also like to thank Guillermo S. Colón-Quintana (University of North Carolina at Chapel Hill), Kathyrn J. Vannoy (University of North Carolina at Chapel Hill), Thomas B. Clarke (University of North Carolina at Chapel Hill), Koun Lim, Ph.D (University of North Carolina at Chapel Hill), and Nicole E. Tarolla, M.S. for helpful discussions.

TOC Graphic:

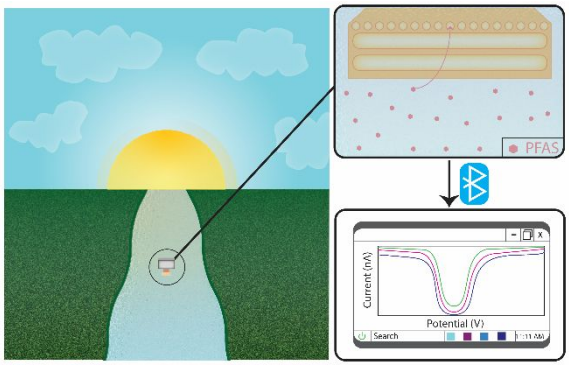

References

1. Prevedouros, K.; Cousins, I. T.; Buck, R. C.; Korzeniowski, S. H., Sources, Fate and Transport of Perfluorocarboxylates. *Environmental Science & Technology* **2006,** *40* (1), 32-44.
2. Kwon, B. G.; Lim, H.-J.; Na, S.-H.; Choi, B.-I.; Shin, D.-S.; Chung, S.-Y., Biodegradation of perfluorooctanesulfonate (PFOS) as an emerging contaminant. *Chemosphere* **2014,** *109*, 221-225.
3. Kim, T.-H.; Lee, S.-H.; Kim, H. Y.; Doudrick, K.; Yu, S.; Kim, S. D., Decomposition of perfluorooctane sulfonate (PFOS) using a hybrid process with electron beam and chemical oxidants. *Chemical Engineering Journal* **2019,** *361*, 1363-1370.
4. Lemal, D. M., Perspective on Fluorocarbon Chemistry. *The Journal of Organic Chemistry* **2004,** *69* (1), 1-11.
5. Domingo, J. L.; Nadal, M., Human exposure to per- and polyfluoroalkyl substances (PFAS) through drinking water: A review of the recent scientific literature. *Environmental Research* **2019,** *177*, 108648.
6. Kucharzyk, K. H.; Darlington, R.; Benotti, M.; Deeb, R.; Hawley, E., Novel treatment technologies for PFAS compounds: A critical review. *Journal of Environmental Management* **2017,** *204*, 757-764.
7. Bao, W.-W.; Qian, Z. M.; Geiger, S. D.; Liu, E.; Liu, Y.; Wang, S.-Q.; Lawrence, W. R.; Yang, B.-Y.; Hu, L.-W.; Zeng, X.-W.; Dong, G.-H., Gender-specific associations between serum isomers of perfluoroalkyl substances and blood pressure among Chinese: Isomers of C8 Health Project in China. *The Science of the total environment* **2017,** *607-608*, 1304-1312.
8. Zeng, Z.; Song, B.; Xiao, R.; Zeng, G.; Gong, J.; Chen, M.; Xu, P.; Zhang, P.; Shen, M.; Yi, H., Assessing the human health risks of perfluorooctane sulfonate by in vivo and in vitro studies. *Environment International* **2019,** *126*, 598-610.
9. Bjork, J. A.; Lau, C.; Chang, S. C.; Butenhoff, J. L.; Wallace, K. B., Perfluorooctane sulfonate-induced changes in fetal rat liver gene expression. *Toxicology* **2008,** *251* (1), 8-20.
10. Blake, B. E.; Pinney, S. M.; Hines, E. P.; Fenton, S. E.; Ferguson, K. K., Associations between longitudinal serum perfluoroalkyl substance (PFAS) levels and measures of thyroid hormone, kidney function, and body mass index in the Fernald Community Cohort. *Environmental Pollution* **2018,** *242*, 894-904.

11. Blake Bevin, E.; Cope Harlie, A.; Hall Samantha, M.; Keys Robert, D.; Mahler Beth, W.; McCord, J.; Scott, B.; Stapleton Heather, M.; Strynar Mark, J.; Elmore Susan, A.; Fenton Suzanne, E., Evaluation of Maternal, Embryo, and Placental Effects in CD-1 Mice following Gestational Exposure to Perfluorooctanoic Acid (PFOA) or Hexafluoropropylene Oxide Dimer Acid (HFPO-DA or GenX). *Environmental Health Perspectives 128* (2), 027006.
12. Temkin, A. M.; Hocevar, B. A.; Andrews, D. Q.; Naidenko, O. V.; Kamendulis, L. M., Application of the Key Characteristics of Carcinogens to Per and Polyfluoroalkyl Substances. *International journal of environmental research and public health* **2020,** *17* (5), 1668.
13. Oliaei, F.; Kriens, D.; Weber, R.; Watson, A., PFOS and PFC releases and associated pollution from a PFC production plant in Minnesota (USA). *Environmental Science and Pollution Research* **2013,** *20* (4), 1977-1992.
14. Cui, J.; Gao, P.; Deng, Y., Destruction of Per- and Polyfluoroalkyl Substances (PFAS) with Advanced Reduction Processes (ARPs): A Critical Review. *Environmental Science & Technology* **2020,** *54* (7), 3752-3766.
15. Winchell, L. J.; Ross, J. J.; Wells, M. J. M.; Fonoll, X.; Norton Jr, J. W.; Bell, K. Y., Per- and polyfluoroalkyl substances thermal destruction at water resource recovery facilities: A state of the science review. *Water Environment Research* **2020,** *n/a* (n/a).
16. Ateia, M.; Alsbaiee, A.; Karanfil, T.; Dichtel, W., Efficient PFAS Removal by Amine-Functionalized Sorbents: Critical Review of the Current Literature. *Environmental Science & Technology Letters* **2019,** *6* (12), 688-695.
17. Kumarasamy, E.; Manning, I. M.; Collins, L. B.; Coronell, O.; Leibfarth, F. A., Ionic Fluorogels for Remediation of Per- and Polyfluorinated Alkyl Substances from Water. *ACS Central Science* **2020,** *6* (4), 487-492.
18. Schultz, M. M.; Barofsky, D. F.; Field, J. A., Quantitative Determination of Fluorotelomer Sulfonates in Groundwater by LC MS/MS. *Environmental Science & Technology* **2004,** *38* (6), 1828-1835.
19. Yoo, H.; Washington, J. W.; Jenkins, T. M.; Ellington, J. J., Quantitative Determination of Perfluorochemicals and Fluorotelomer Alcohols in Plants from Biosolid-Amended Fields using LC/MS/MS and GC/MS. *Environmental Science & Technology* **2011,** *45* (19), 7985-7990.
20. Teymourian, H.; Barfidokht, A.; Wang, J., Electrochemical glucose sensors in diabetes management: an updated review (2010–2020). *Chemical Society Reviews* **2020,** *49* (21), 7671-7709.
21. Wang, Y.; Luo, J.; Liu, J.; Sun, S.; Xiong, Y.; Ma, Y.; Yan, S.; Yang, Y.; Yin, H.; Cai, X., Label-free microfluidic paper-based electrochemical aptasensor for ultrasensitive and simultaneous multiplexed detection of cancer biomarkers. *Biosensors and Bioelectronics* **2019,** *136*, 84-90.
22. Selvolini, G.; Marrazza, G., MIP-Based Sensors: Promising New Tools for Cancer Biomarker Determination. *Sensors (Basel, Switzerland)* **2017,** *17* (4), 718.
23. Dick, J. E.; Hilterbrand, A. T.; Strawsine, L. M.; Upton, J. W.; Bard, A. J., Enzymatically enhanced collisions on ultramicroelectrodes for specific and rapid detection of individual viruses. *Proceedings of the National Academy of Sciences* **2016,** *113* (23), 6403-6408.
24. Glasscott, M. W.; Vannoy, K. J.; Iresh Fernando, P. U. A.; Kosgei, G. K.; Moores, L. C.; Dick, J. E., Electrochemical sensors for the detection of fentanyl and its analogs: Foundations and recent advances. *TrAC Trends in Analytical Chemistry* **2020,** *132*, 116037.
25. Kazemi, R.; Potts, E. I.; Dick, J. E., Quantifying Interferent Effects on Molecularly Imprinted Polymer PFAS Sensors. *Analytical Chemistry* **2020**.
26. Clark, R. B.; Dick, J. E., Electrochemical Sensing of Perfluorooctanesulfonate (PFOS) Using Ambient Oxygen in River Water. *ACS Sensors* **2020,** *5* (11), 3591-3598.
27. Karimian, N.; Stortini, A. M.; Moretto, L. M.; Costantino, C.; Bogialli, S.; Ugo, P., Electrochemosensor for Trace Analysis of Perfluorooctanesulfonate in Water Based on a Molecularly Imprinted Poly(o-phenylenediamine) Polymer. *ACS Sensors* **2018,** *3* (7), 1291-1298.
28. Glasscott, M. W.; Vannoy, K. J.; Kazemi, R.; Verber, M. D.; Dick, J. E., μ-MIP: Molecularly Imprinted Polymer-Modified Microelectrodes for the Ultrasensitive Quantification of GenX (HFPO-DA) in River Water. *Environmental Science & Technology Letters* **2020,** *7*, 489-495.
29. Jafari, S.; Dehghani, M.; Nasirizadeh, N.; Azimzadeh, M., An azithromycin electrochemical sensor based on an aniline MIP film electropolymerized on a gold nano urchins/graphene oxide modified glassy carbon electrode. *Journal of Electroanalytical Chemistry* **2018,** *829*, 27-34.
30. Waffo, A. F. T.; Yesildag, C.; Caserta, G.; Katz, S.; Zebger, I.; Lensen, M. C.; Wollenberger, U.; Scheller, F. W.; Altintas, Z., Fully electrochemical MIP sensor for artemisinin. *Sensors and Actuators B: Chemical* **2018,** *275*, 163-173.
31. Yarman, A.; Scheller, F. W., The first electrochemical MIP sensor for tamoxifen. *Sensors (Basel, Switzerland)* **2014,** *14* (5), 7647-7654.
32. Ayankojo, A. G.; Reut, J.; Ciocan, V.; Öpik, A.; Syritski, V., Molecularly imprinted polymer-based sensor for electrochemical detection of erythromycin. *Talanta* **2020,** *209*, 120502.
33. Furst, A. L.; Hoepker, A. C.; Francis, M. B., Quantifying Hormone Disruptors with an Engineered Bacterial Biosensor. *ACS Central Science* **2017,** *3* (2), 110-116.
34. Ruan, C.; Yang, L.; Li, Y., Immunobiosensor Chips for Detection of Escherichia coli O157:H7 Using Electrochemical Impedance Spectroscopy. *Analytical Chemistry* **2002,** *74* (18), 4814-4820.
35. Bard, A. J.; Zhou, H.; Kwon, S. J., Electrochemistry of Single Nanoparticles via Electrocatalytic Amplification. *Israel Journal of Chemistry* **2010,** *50* (3), 267-276.
36. Dick, J. E.; Hilterbrand, A. T.; Boika, A.; Upton, J. W.; Bard, A. J., Electrochemical detection of a single cytomegalovirus at an ultramicroelectrode and its antibody anchoring. *Proceedings of the National Academy of Sciences* **2015,** *112* (17), 5303-5308.
37. Zhou, M.; Dick, J. E.; Bard, A. J., Electrodeposition of Isolated Platinum Atoms and Clusters on Bismuth—Characterization and Electrocatalysis. *Journal of the American Chemical Society* **2017,** *139* (48), 17677-17682.
38. Zhou, M.; Bao, S.; Bard, A. J., Probing Size and Substrate Effects on the Hydrogen Evolution Reaction by Single Isolated Pt Atoms, Atomic Clusters, and Nanoparticles. *Journal of the American Chemical Society* **2019,** *141* (18), 7327-7332.
39. Jin, Z.; Bard, A. J., Atom-by-atom electrodeposition of single isolated cobalt oxide molecules and clusters for studying the oxygen evolution reaction. *Proceedings of the National Academy of Sciences* **2020,** *117* (23), 12651.

40. Shumyantseva, V. V.; Bulko, T. V.; Sigolaeva, L. V.; Kuzikov, A. V.; Archakov, A. I., Electrosynthesis and binding properties of molecularly imprinted poly-o-phenylenediamine for selective recognition and direct electrochemical detection of myoglobin. *Biosensors and Bioelectronics* **2016,** *86*, 330-336.
41. Grothe, R. A.; Lobato, A.; Mounssef, B.; Tasić, N.; Braga, A. A. C.; Maldaner, A. O.; Aldous, L.; Paixão, T. R. L. C.; Gonçalves, L. M., Electroanalytical profiling of cocaine samples by means of an electropolymerized molecularly imprinted polymer using benzocaine as the template molecule. *Analyst* **2021,** *146* (5), 1747-1759.
42. Weng, C.-H.; Yeh, W.-M.; Ho, K.-C.; Lee, G.-B., A microfluidic system utilizing molecularly imprinted polymer films for amperometric detection of morphine. *Sensors and Actuators B: Chemical* **2007,** *121* (2), 576-582.
43. Motia, S.; Tudor, I. A.; Madalina Popescu, L.; Piticescu, R. M.; Bouchikhi, B.; El Bari, N., Development of a novel electrochemical sensor based on electropolymerized molecularly imprinted polymer for selective detection of sodium lauryl sulfate in environmental waters and cosmetic products. *Journal of Electroanalytical Chemistry* **2018,** *823*, 553-562.
44. Apodaca, D. C.; Pernites, R. B.; Ponnapati, R.; Del Mundo, F. R.; Advincula, R. C., Electropolymerized Molecularly Imprinted Polymer Film: EIS Sensing of Bisphenol A. *Macromolecules* **2011,** *44* (17), 6669-6682.
45. Zhang, X.; Peng, Y.; Bai, J.; Ning, B.; Sun, S.; Hong, X.; Liu, Y.; Liu, Y.; Gao, Z., A novel electrochemical sensor based on electropolymerized molecularly imprinted polymer and gold nanomaterials amplification for estradiol detection. *Sensors and Actuators B: Chemical* **2014,** *200*, 69-75.
46. Aghaei, A.; Milani Hosseini, M. R.; Najafi, M., A novel capacitive biosensor for cholesterol assay that uses an electropolymerized molecularly imprinted polymer. *Electrochimica Acta* **2010,** *55* (5), 1503-1508.
47. Crapnell, R. D.; Hudson, A.; Foster, C. W.; Eersels, K.; Grinsven, B. V.; Cleij, T. J.; Banks, C. E.; Peeters, M., Recent Advances in Electrosynthesized Molecularly Imprinted Polymer Sensing Platforms for Bioanalyte Detection. *Sensors (Basel)* **2019,** *19* (5).
48. Udomsap, D.; Branger, C.; Culioli, G.; Dollet, P.; Brisset, H., A versatile electrochemical sensing receptor based on a molecularly imprinted polymer. *Chemical communications (Cambridge, England)* **2014,** *50*, 7488.
49. Urban, P. L., Please Avoid Plotting Analytical Response against Logarithm of Concentration. *Analytical Chemistry* **2020,** *92* (15), 10210-10212.
50. Alizadeh, T.; Atashi, F.; Ganjali, M. R., Molecularly imprinted polymer nano-sphere/multi-walled carbon nanotube coated glassy carbon electrode as an ultra-sensitive voltammetric sensor for picomolar level determination of RDX. *Talanta* **2019,** *194*, 415-421.
51. Cieplak, M.; Kutner, W., Artificial Biosensors: How Can Molecular Imprinting Mimic Biorecognition? *Trends Biotechnol* **2016,** *34* (11), 922-941.
52. Azizi, A.; Bottaro, C. S., A critical review of molecularly imprinted polymers for the analysis of organic pollutants in environmental water samples. *Journal of Chromatography A* **2020,** *1614*, 460603.
53. Patel, H.; Vashi, R. T., Chapter 2 - Characterization of Textile Wastewater. In *Characterization and Treatment of Textile Wastewater*, Patel, H.; Vashi, R. T., Eds. Elsevier: Boston, 2015; pp 21-71.
54. Bard, A. J.; Faulkner, L. R., *Electrochemical Methods: Fundamentals and Applications*. Wiley: 2000.
55. Clark, R. B.; Glasscott, M. W.; Verber, M. D.; DeMartino, J. C.; Netchaev, A.; Ray, J. D.; Brown, E. W.; Alberts, E.; Fernando, P. U. A. I.; Moores, L. C.; Dick, J. E., A Generalized Potentiostat Adaptor for Multiplexed Electroanalysis. *Analytical Chemistry* **2021**.
56. Ordeig, O.; del Campo, J.; Muñoz, F. X.; Banks, C. E.; Compton, R. G., Electroanalysis Utilizing Amperometric Microdisk Electrode Arrays. *Electroanalysis* **2007,** *19* (19-20), 1973-1986.
57. Spira, M. E.; Hai, A., Multi-electrode array technologies for neuroscience and cardiology. *Nature Nanotechnology* **2013,** *8* (2), 83-94.
58. Merletti, R.; Farina, D.; Gazzoni, M., The linear electrode array: a useful tool with many applications. *J. Electromyogr. Kinesiol.* **2003,** *13* (1), 37-47.
59. Diamond, D., Progress in sensor array research. *Electroanalysis* **1993,** *5* (9-10), 795-802.
60. Dryden, M. D. M.; Wheeler, A. R., DStat: A Versatile, Open-Source Potentiostat for Electroanalysis and Integration. *PLOS ONE* **2015,** *10* (10), e0140349.
61. Cordova-Huaman, A. V.; Jauja-Ccana, V. R.; La Rosa-Toro, A., Low-cost smartphone-controlled potentiostat based on Arduino for teaching electrochemistry fundamentals and applications. *Heliyon* **2021,** *7* (2), e06259.
62. Glasscott, M. W.; Verber, M. D.; Hall, J. R.; Pendergast, A. D.; McKinney, C. J.; Dick, J. E., SweepStat: A Build-It-Yourself, Two-Electrode Potentiostat for Macroelectrode and Ultramicroelectrode Studies. *Journal of Chemical Education* **2020,** *97* (1), 265-270.